ACS APPLIED MATERIALS & INTERFACES

Research Article

www.acsami.org

Dual Functional Sensing Mechanism in SnO_2–ZnO Core–Shell Nanowires

Sun-Woo Choi,[†] Akash Katoch,[†] Gun-Joo Sun,[†] Jae-Hun Kim,[†] Soo-Hyun Kim,[‡] and Sang Sub Kim*[,†]

[†]Department of Materials Science and Engineering, Inha University, Incheon 402-751, Republic of Korea

[‡]School of Materials Science and Engineering, Yeungnam University, Gyeongsangbuk-do 712-749, Republic of Korea

Supporting Information

ABSTRACT: We report a dual functional sensing mechanism for ultrasensitive chemoresistive sensors based on SnO_2–ZnO core–shell nanowires (C–S NWs) for detection of trace amounts of reducing gases. C–S NWs were synthesized by a two-step process, in which core SnO_2 nanowires were first prepared by vapor–liquid–solid growth and ZnO shell layers were subsequently deposited by atomic layer deposition. The radial modulation of the electron-depleted shell layer was accomplished by controlling its thickness. The sensing capabilities of C–S NWs were investigated in terms of CO, which is a typical reducing gas. At an optimized shell thickness, C–S NWs showed the best CO sensing ability, which was quite superior to that of pure SnO_2 nanowires without a shell. The dual functional sensing mechanism is proposed as the sensing mechanism in these nanowires and is based on the combination of the radial modulation effect of the electron-depleted shell and the electric field smearing effect.

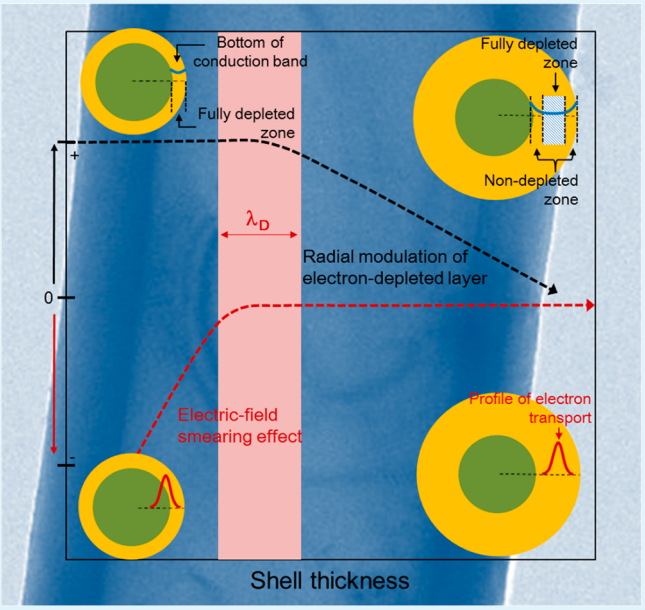

KEYWORDS: *core–shell, nanowires, gas sensor, SnO_2–ZnO, sensing mechanism*

1. INTRODUCTION

The development of fast, accurate, and reliable sensors that can detect hazardous chemical species is a major demand of the science and technology community to prevent the pollution of our environment. Over the past several years, various types of materials have been tested as sensing materials. Oxide nanomaterials in the forms of nanowires (NWs), nanorods, and nanofibers have attracted a growing amount of attention for use as promising sensing materials because of their useful properties, including a large surface area, fast diffusion kinetics, and high intrinsic modulation of electrical transport.[1−5]

One of the most important issues in the field of chemoresistive sensors is the sufficient improvement of their sensing performance for the detection of extremely low concentrations of chemical species. One route to achieving this is the application of core–shell (C–S) heterostructures.[6−9] In such structures, a heterojunction is created at the interface between the core and shell and can play a role in enhancing the sensing capability, making it better than those of single-structure counterparts.[10−12] A literature survey[13,14] indeed suggests that the use of C–S structures results in enhanced sensing performance, particularly when the shell thickness is shorter than or equivalent to the Debye length of the shell material.

Very recently, the sensing mechanism of SnO_2–ZnO C–S nanofibers was systematically investigated.[14] In that investigation, only the radial modulation of the electron-depleted shell layer was thought to be responsible for the improvement in the sensing properties of the C–S structures. In addition, it was suggested that C–S nanofibers comprising dissimilar materials having different energy band structures can be an effective sensing platform for the detection of low concentrations of reducing gases when the shell thickness is equivalent to the Debye length. However, individual oxide nanofibers are usually composed of nanosized grains (or nanograins).[15−19] They are likely to greatly influence the sensing properties of oxide nanofibers.[18,19] From that point of view, nanofibers are not a perfect material system for investigating the sensing mechanism of C–S structures because the presence of nanograins may complicate the sensing mechanism, making it

Received: February 22, 2014
Accepted: May 17, 2014
Published: May 17, 2014

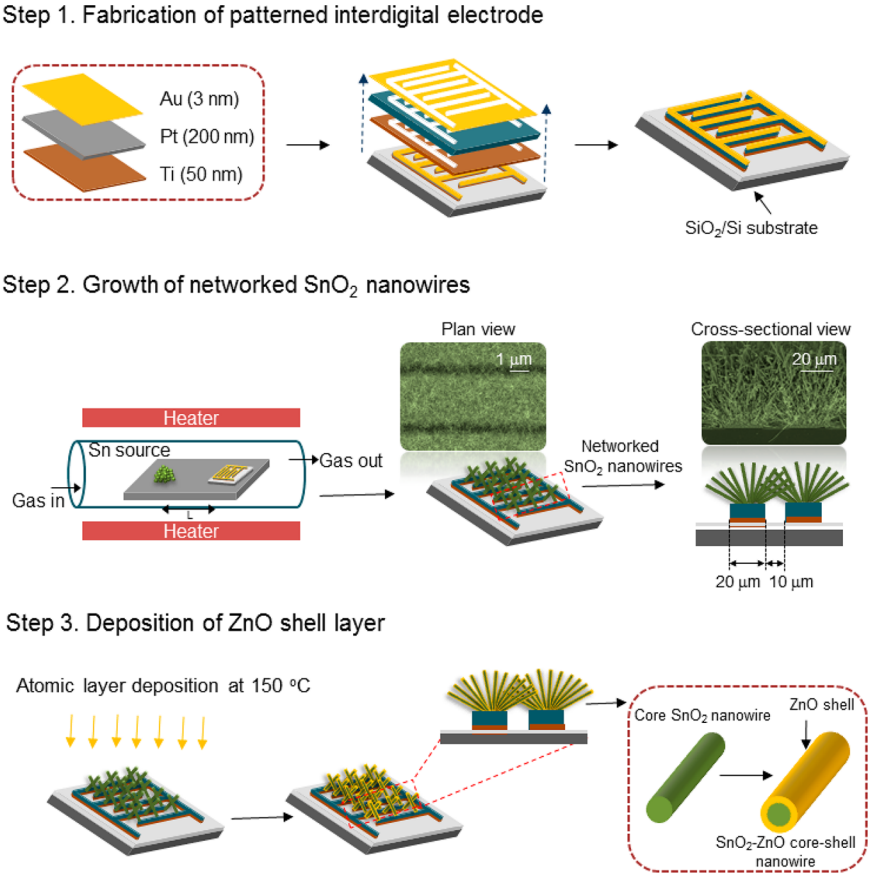

Figure 1. Schematics and corresponding real images of the fabrication sequence of sensors based on SnO_2–ZnO C–S NWs.

difficult to identify the mechanism originating from only the C–S structures. Instead of C–S nanofibers, C–S NWs are more suitable for revealing the underlying sensing mechanism operating in C–S structures because the possibility of incorporating other disturbing sources like nanograins can be excluded.

In this work, the sensing mechanism of SnO_2–ZnO C–S NWs was investigated for the purpose of clearly understanding the sensing mechanism operating in C–S structures. C–S NWs were synthesized by sequentially employing vapor-phase growth and atomic layer deposition (ALD) techniques. The sensing performances of the NWs were tested as a function of the ZnO shell thickness in terms of CO, which was employed as a representative reducing gas. A dual functional sensing mechanism based on the combination of the radial modulation effect in the electron-depleted shell and the field smearing effect was suggested as the responsible mechanism of the C–S NWs.

2. EXPERIMENTAL SECTION

The synthesis of SnO_2–ZnO C–S NWs involved three steps. In the first step, patterned interdigital electrodes (PIEs) were fabricated on SiO_2-grown Si(100) substrates by using a conventional photolithographic process. The electrode used was a Au (3 nm)/Pt (100 nm)/Ti (100 nm) layer that had sequentially been deposited by a sputtering method. The Au top layer played the role of a catalytic layer for the selective growth of SnO_2 nanowires. In the second step, networked SnO_2 nanowires were selectively grown on a catalytic Au pad layer by using the well-known vapor–liquid–solid method. SnO_2 nanowires selectively grown on the PIEs became tangled with each other in the electrode spacing, consequently producing networked junctions. Both the experimental procedure for fabricating networked SnO_2 nanowires and the effects of the length and diameter of nanowires on gas sensing properties have been described in detail previously.[20]

In the third step, ZnO shells were deposited on networked SnO_2 nanowires by ALD using a traveling wave-type ALD reactor (Lucida D100, NCD technology), which is a particularly effective method for synthesizing a uniform, conformal layer on irregularly shaped substrates. Diethylzinc [$Zn(C_2H_5)_2$ or DEZn] and water vapor (H_2O) were used as a precursor and reactant, respectively. The DEZn and water vapor were contained in a canister kept at 10 °C. The temperature and pressure of the reactor were maintained at 150 °C and ~1 Torr, respectively. In these investigations, the basic pulsing conditions were precursor pulsing for 2 s, reactant pulsing for 2 s, and purging for 10 s, which are found to be enough to guarantee the self-limited growth of the ZnO film. Between the precursor pulsing and the reactant pulsing, a purging process was conducted with 100 standard cubic centimeters per minute (sccm) of N_2; the sequence of precursor pulsing, precursor purging, reactant pulsing, and then reactant purging occurs in each ALD cycle. In this way, SnO_2–ZnO C–S NWs with uniform shell thicknesses were synthesized. By changing the number of ALD cycles, we successfully controlled the ZnO shell thickness so that it was in the range 3.5–95 nm. The experimental procedure for ALD was described previously.[21] The schematics and corresponding real images of the fabrication sequence for the sensors based on C–S NWs are shown in Figure 1.

The microstructure and phase of the synthesized C–S NWs were examined by field emission scanning electron microscopy (FE-SEM) and transmission electron microscopy (TEM) and by X-ray diffraction (XRD), respectively. The sensing capabilities of the C–S NW sensors were investigated as a function of the shell thickness using various reducing gases, namely, CO, C_6H_6, and C_7H_8, as well as a representative oxidizing gas, NO_2. The sensing measurements were taken at 300 °C using a homemade gas dilution and sensing measurement system after preliminary experiments to determine the optimal operating temperature. The detailed experimental procedure

for the sensing measurements was described previously.[22,23] The sensor response (R) for reducing (or oxidizing) gases was estimated using the equation $R = R_a/R_g$ (or R_g/R_a), where R_a and R_g are the resistances in the absence and presence of the target gas, respectively.

3. RESULTS

As the schematic illustrations shown in Figure 1 demonstrate, by applying a suitable spacing of the PIE, one can obtain a well-networked propensity of SnO_2 NWs. Plane-view and cross-sectional FE-SEM images taken from a part of networked SnO_2 NWs on neighboring PIEs are included in the figure, clearly revealing the entangled condition of SnO_2 NWs that can play the role of an electrical transport pathway.

On these networked SnO_2 NWs, ZnO shell layers were deposited via ALD. Panels a–f of Figure 2 display the morphologies of SnO_2–ZnO C–S NWs with various shell thicknesses ranging from 0 to 95 nm. For the sake of comparison, a microstructure of pristine SnO_2 NWs is also included in Figure 2a. The average diameter of the pristine SnO_2 NWs was ~70–90 nm. The FE-SEM images clearly show that the ALD process resulted in uniform, conformal coverage of the ZnO shell layers on the core SnO_2 NWs even at a very small shell thickness of 3.5 nm. In sharp contrast to C–S nanofibers[14] that are composed of nanograins, the C–S NWs do not show any grains, being seemingly single-crystalline. This feature will allow us to interpret more clearly the underlying sensing mechanism in various C–S structures. It is evident that the ZnO shell thickness gradually increases with an increase in the number of ALD cycles. The shell thickness can be calculated from the FE-SEM images and is summarized in Figure 3, showing the relationship between the shell thickness and the number of ALD cycles. The slope is 0.16 nm/cycle.

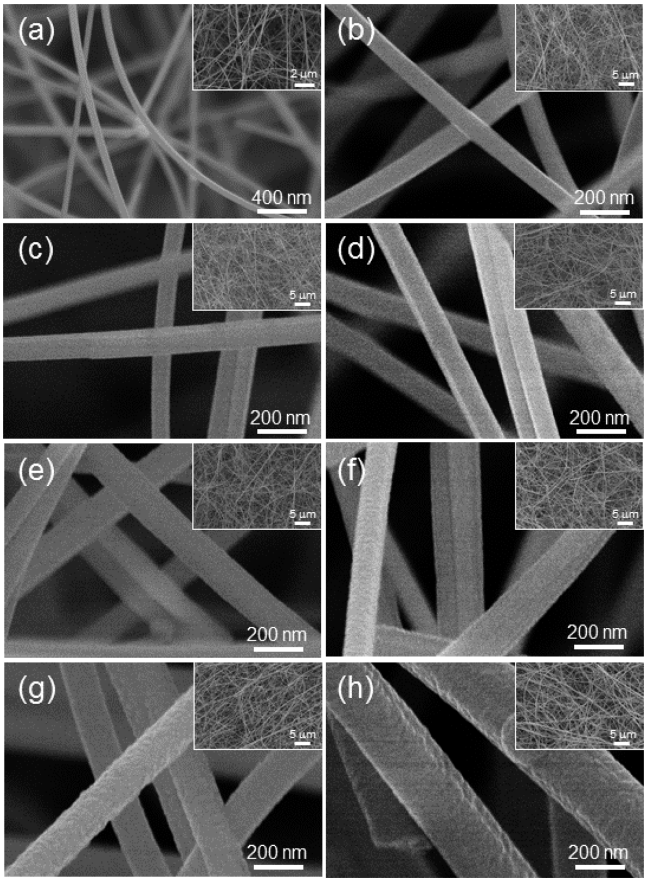

Figure 2. Typical morphologies of SnO_2–ZnO C–S NWs with various shell thicknesses ranging from 0 to 95 nm: (a) 0, (b) 3.5, (c) 7.5, (d) 13, (e) 20, (f) 25, (g) 40, and (h) 95 nm. Note that for the sake of comparison, the microstructure of pristine SnO_2 NWs is included in panel a. The insets are the corresponding low-magnification FE-SEM images, showing the overall features of C–S NWs.

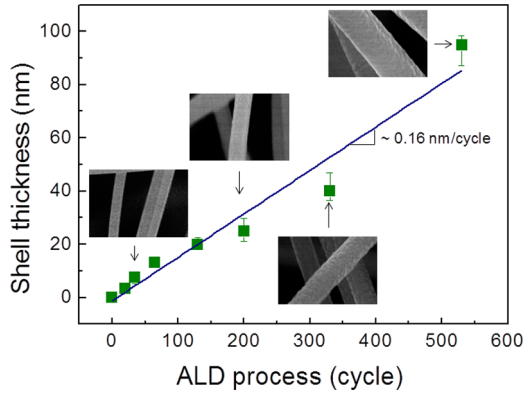

Figure 3. Relationship between the shell thickness and the number of ALD cycles. The slope is 0.16 nm/cycle.

The microstructure of SnO_2–ZnO C–S NWs was further investigated by TEM observations. Figure 4a shows a high-magnification TEM image of a sample with a shell thickness of 25 nm, again demonstrating that the ZnO shell layer uniformly covered the SnO_2 core NWs. The results of elemental line scans with respect to O, Sn, and Zn are displayed in Figure 4b. It can be seen that O and Zn are distributed in the whole volume of an individual nanowire. In sharp contrast, Sn is confined to only the core region. This spatial distribution of O, Sn, and Zn in C–S NWs definitely demonstrates the formation of the ZnO shell layer on the SnO_2 core NWs.

XRD was used to identify the phases of SnO_2–ZnO C–S NWs. The results are shown in Figure S1 of the Supporting Information. The XRD patterns were recorded using a Cu Kα (1.5418 Å) source. The patterns exhibit both SnO_2 and ZnO phases. The SnO_2 tetragonal rutile phase has lattice parameters a = 4.73 Å and c = 3.18 Å (JCPDS Card No. 88-0287), whereas the wurtzite phase of ZnO has lattice parameters a = 3.24 Å and c = 5.205 Å (JCPDS Card No. 89-0511), again confirming the formation of SnO_2–ZnO C–S NWs. It is worth noting that the intensity of the peaks corresponding to the ZnO phase increases with an increasing shell thickness, which is due to a larger amount of ZnO being exposed to X-rays. This again confirms the proportional increase in the ZnO shell thickness with an increasing number of ALD cycles.

The sensing performances of SnO_2–ZnO C–S NW sensors with various shell thicknesses were investigated using various reducing gases, namely, CO, C_6H_6, and C_7H_8, as well as a representative oxidizing gas, NO_2. In our earlier work,[14] C–S structures were found to be beneficial for detecting reducing gases rather than oxidizing ones. In Figure S2 of the Supporting Information, measured resistance curves for the gases mentioned above are shown. All the sensors clearly track

dx.doi.org/10.1021/am501107c | ACS Appl. Mater. Interfaces 2014, 6, 8281–8287

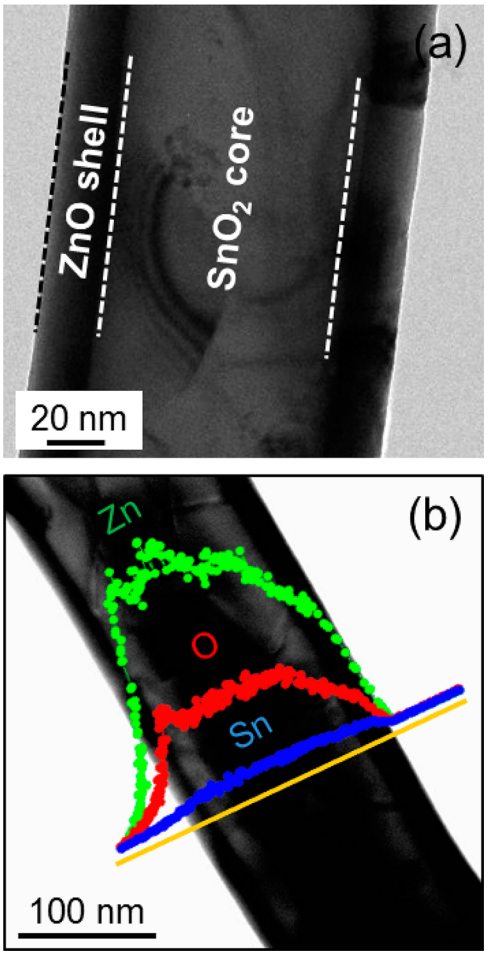

Figure 4. (a) High-magnification TEM image of a SnO_2–ZnO C–S NW with a shell thickness of 25 nm. (b) Results of elemental line scans with respect to O, Sn, and Zn.

changes in the gas environment. The resistance of the sensors decreases when reducing gases are supplied, and it increases when their supply is stopped and air is introduced. This behavior can be explained by the well-known *n*-type semiconductor sensing mechanism.[24] In addition, the resistance curves show the opposite behaviors with regard to NO_2, as expected. One important feature observed in Figure S2 of the Supporting Information is that the sensor response is highly dependent on the shell thickness.

To more clearly reveal the effect of the shell thickness on the sensing properties, the gas responses to a concentration of 1 ppm are summarized in Figure 5. The response of the pure SnO_2 NW sensor without a ZnO shell layer is gradually enhanced by the formation of a ZnO shell layer for all reducing gases. The C–S NW sensor with a shell thickness of 40 nm shows the best response to all the tested reducing gases. However, a further increase in shell thickness greatly weakens the response. In other words, the C–S NW sensors with shells having thickness both smaller and larger than the critical thickness show inferior responses, suggesting that the shell thickness needs to be optimized to obtain superior sensing abilities for C–S NW sensors. Another point that needs to be mentioned is that the presence of the ZnO shell layers rather weakens the sensing properties for oxidizing gases.

4. DISCUSSION

In a previous work[14] regarding SnO_2–ZnO C–S nanofiber sensors, a model for a possible sensing mechanism has been proposed only on the basis of the radial modulation of electron-depleted shells. The model suggests that C–S structures comprising dissimilar materials having different energy band structures can be effective sensing platforms for the detection of low concentrations of reducing gases when the shell thickness is equivalent to the Debye length of the shell layer. However, in C–S nanofibers, individual C–S fibers consist of nanosized grains, which may dominantly determine the sensing abilities of these nanofibers. Another point that should be noted here is that in C–S nanofibers, the shell layers may not completely cover the entire surface of the core nanofibers, particularly for thin shell layers. Such a partially covered shell layer will prevent us from straightforwardly understanding the sensing mechanism involved in C–S structures. For these reasons, instead of C–S nanofibers prepared in the previous work,[14] SnO_2–ZnO C–S NWs prepared in this study are more likely to be a suitable material system for exploring the underlying sensing mechanism in C–S structures. That is, in SnO_2–ZnO C–S NW sensors, one can exclude the possibility of the effects of nanosized grains because both the core and shell are basically single-crystalline structures without any nanograins. Moreover, the ZnO shell layer coats the surface of SnO_2 core NWs uniformly and completely even for a very small thickness. This is different from the case of C–S nanofibers in which the shell layer is partially covered at very small thicknesses.

According to the results shown in Figure 6, SnO_2–ZnO C–S NWs with a shell thickness of 40 nm showed the best response to reducing gases such as CO, C_6H_6, and C_7H_8. On the other hand, the formation of shell layers weakened the NO_2 sensing performances of core NWs. These results seemingly appear to be the same in nature as those for C–S nanofibers.[14] However, in the case of C–S nanofibers, when the shells are thinner than the Debye length, they are thought to partially coat the core nanofibers. This partial coverage has been suggested as being responsible for lower gas responses. In principle, in any kind of C–S structures, the shell layer will be fully electron-depleted by both the adsorption of oxygen species on its surface and the electron flow at the core–shell interface when the shell thickness is equal to or smaller than the Debye length of the shell layer. In this case, resistance modulation due to the release of captured electrons to the shell layer during the supply of reducing gases must be nearly equal for all C–S structures when the shell thickness is equal to or smaller than the Debye length of the shell layer. This explanation based on the radial modulation of the electron-depleted shell layer is described in detail in a previous report.[14] However, it is apparent that the SnO_2–ZnO C–S NWs with ZnO shell layers thinner than the Debye length reveal increased resistance modulation with an increasing shell thickness up to the Debye length, as shown in Figures 5 and 6. This contradicts the expectation based on the mechanism on the radial modulation of the electron-depleted shell layer. Therefore, another factor needs to be considered to account for the obtained sensing results.

In C–S NWs, when the shell thickness is smaller than or comparable to the Debye length (λ_D) of the shell material, the shell layer will be completely electron-depleted in air by the adsorption of oxygen species. λ_D for an oxide material can be calculated by the following equation:[25]

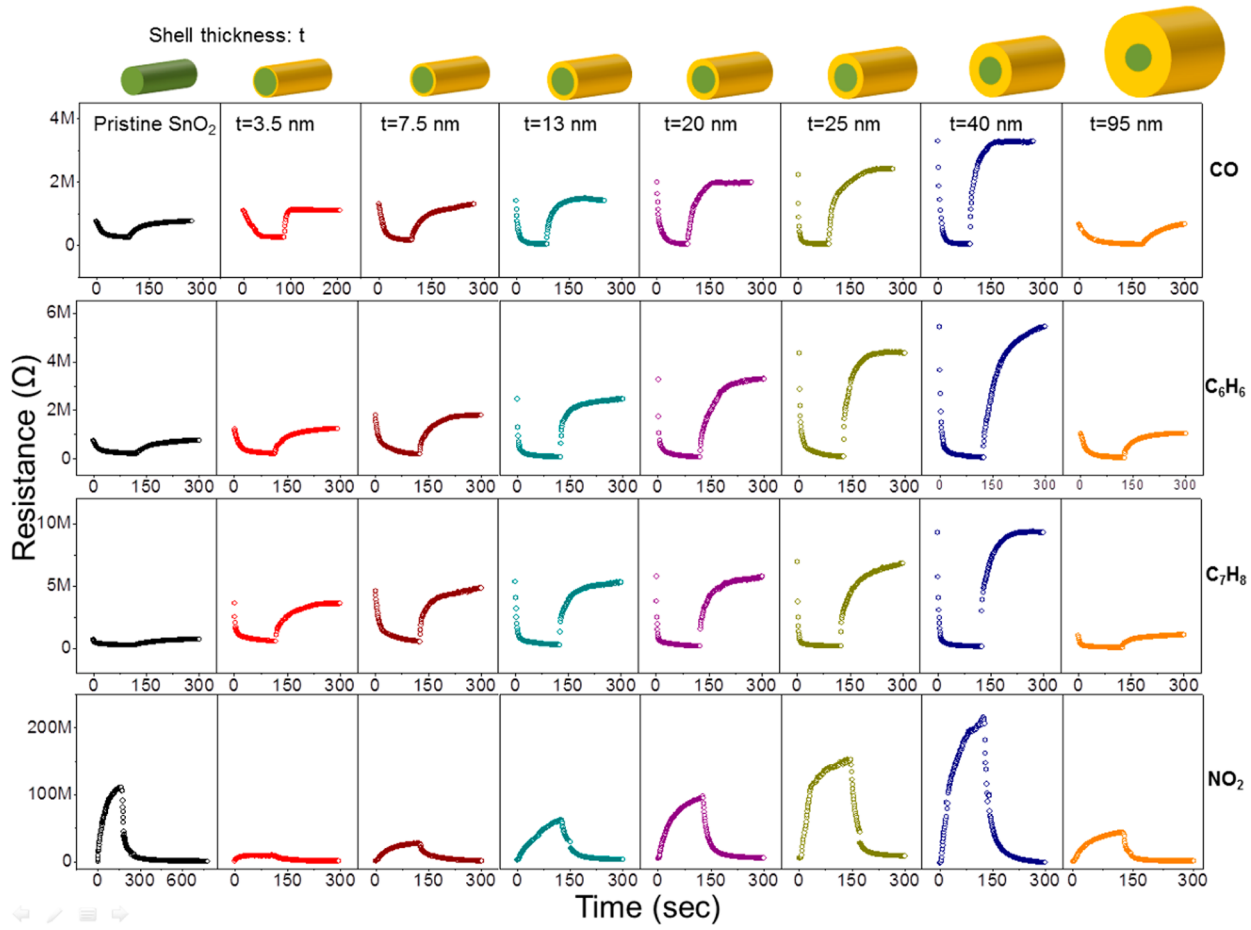

Figure 5. Responses of the SnO_2–ZnO C–S NWs with various shell thickness to 1 ppm CO, C_6H_6, C_7H_8, and NO_2 gases.

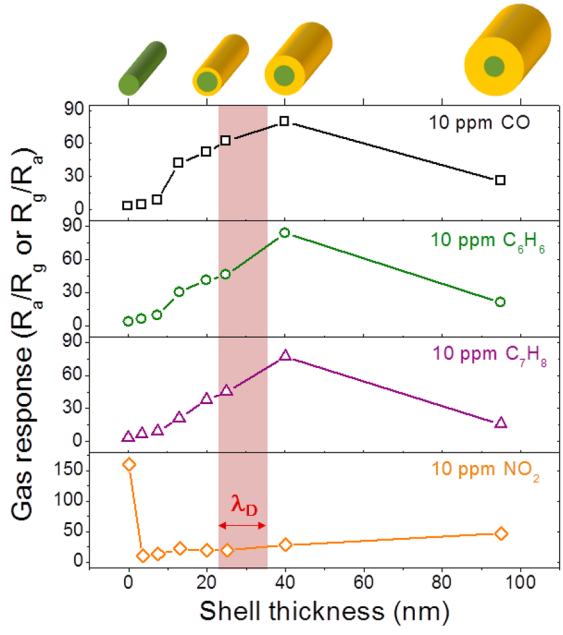

Figure 6. Summary of gas responses of SnO_2–ZnO C–S NWs to 10 ppm gases as a function of shell thickness.

$$\lambda_D = \sqrt{\frac{\varepsilon k T}{q^2 n_c}} \quad (1)$$

where ε, k, T, q, and n_c are the static dielectric constant, Boltzmann's constant, the absolute temperature, the electrical charge, and the carrier charge concentration, respectively. According to eq 1, the λ_D value for bulk ZnO at 300 °C is estimated to be in the range ~22–35 nm.[26,27] In addition, ZnO and SnO_2 have a type II band alignment (see Figure S3 of the Supporting Information);[28,29] consequently, an electron flow takes place at the interface from the ZnO shell layer to the SnO_2 core until the built-up electric field prevents it. This will intensify the electron depletion state in the ZnO shell layer.

The creation of the electron-depleted shell layer, which is electrically resistive, increases the resistance of C–S NWs, as is shown in Figure 7. One important feature is that the sensor resistance of C–S NWs is larger than that of pristine NWs, which indicates that the formation of shell layers leads to an increase in sensor resistance. This increase in resistance definitely indicates that a dominant electrical transport pathway is localized in the vicinity of the shell layer. In case the electrical pathway is evenly distributed along the cross-sectional area of C–S NWs, the creation of a highly resistive electron-depleted shell layer does not significantly influence the resistance of C–S NWs because the core area remains the same irrespective of the presence of a resistive shell layer. However, if electrical transport is fully confined to only the shell layer, the sensor resistance of C–S NWs should be similar irrespective of the variation in the shell thickness if it is thinner than the Debye length of 22–35 nm. However, the observed results rather indicate that electrical transport is not fully localized only in the shell layer, especially when the thickness of the shell layer is

dx.doi.org/10.1021/am501107c | ACS Appl. Mater. Interfaces 2014, 6, 8281–8287

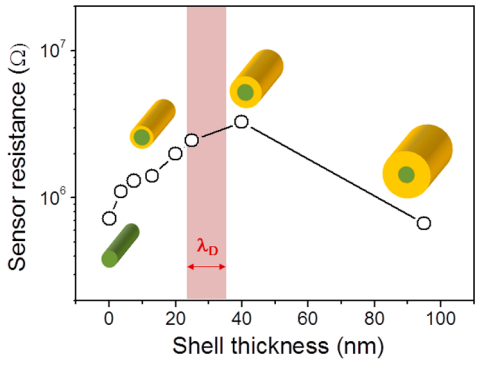

Figure 7. Resistance of SnO_2–ZnO C–S NWs as a function of shell thickness.

smaller than the Debye length. This implies that a smearing effect acts on thin shell layers. In the case of very thin shell layers, electrical transport occurs in the shell and core. As the shell becomes thicker, the transport becomes confined mostly to the shell layer.

As shown in Figure 8, the following scenario is suggested for the sensing mechanism of C–S NWs. The degree of resistance modulation originating from the radial modulation of the electron-depleted shell layer varies according to the shell thickness, as shown in Figure 8a. This is the sensing mechanism described in detail in a previous report.[14] Figure 8b schematically illustrates another sensing mechanism called the electric field smearing effect. When a shell layer thinner than the Debye length is formed on a core material, electrical transport occurs both in the shell layer and around the core at the core–shell interface because the transport will not be confined only to the shell layer. This merely partially increases resistance modulation when the C–S NWs are exposed to reducing gases because electrical transport occurs only partially in the shell layer, which is a fully electrically depleted region. Namely, although the shell layer that is fully electron-depleted will experience a large resistance modulation, a substantial portion of electron transport will also take place through the inner core nanowire, consequently resulting in a marginal resistance modulation for the whole C–S NWs. In contrast, for a shell layer with a thickness equal to or larger than the Debye length, electrical transport will be mostly confined to the shell layer, not smeared to the core region. In this case, the smearing effect will vanish, and the resistance modulation of the C–S NWs by reducing gases will be determined only by the radial modulation of the electron-depleted layer. The two effects mentioned above contribute to the gas response in an additive fashion, consequently leading to Figure 8c. This behavior of resistance modulation (that is, response) as a function of shell thickness is in good agreement with the observed results shown in Figure 6. At this stage, it is not possible to quantify the contribution of the smearing effect in the total resistance modulation. A systematic study based on impedance spectroscopy may reveal more clearly the contributions from the smearing effect and the radial modulation effect of the electron-depleted layer, which needs to be performed in the future.

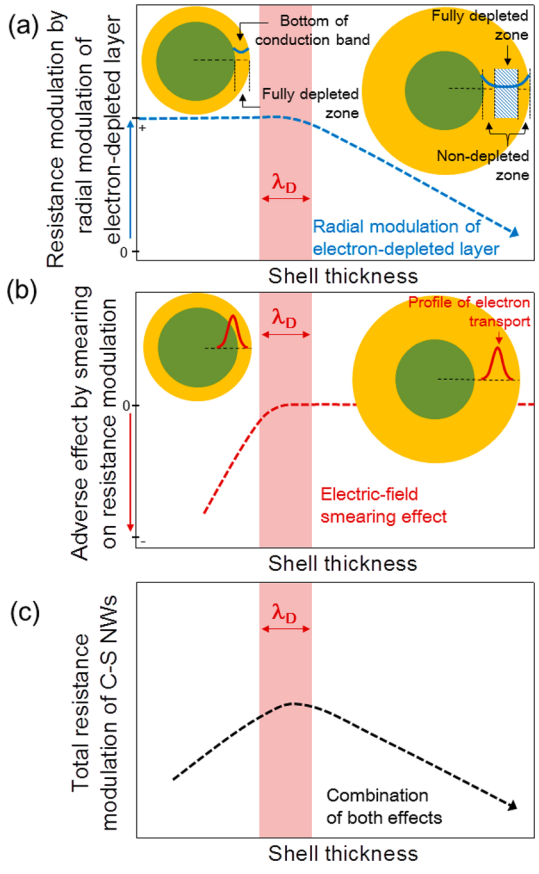

Figure 8. Conceptual description showing the dual functional sensing mechanism of C–S NWs: (a) resistance modulation by radial modulation of the electron-depleted shell layer, (b) adverse effect by smearing on resistance modulation, and (c) total resistance modulation of C–S NWs by a combination of both effects.

5. CONCLUSIONS

We have investigated the sensing mechanism operating in SnO_2–ZnO C–S NWs that are particularly ultrasensitive for the detection of trace amounts of reducing gases. C–S NWs were synthesized by a two-step process: core SnO_2 nanowires were prepared by vapor–liquid–solid growth, and ZnO shell layers were subsequently deposited by ALD. A dual functional sensing mechanism was found to be the sensing mechanism and was based on the contribution of the radial modulation effect of the electron-depleted shell and the electric field smearing effect.

■ ASSOCIATED CONTENT

Ⓢ Supporting Information

Additional details about X-ray diffraction (XRD), resistance curves for SnO_2–ZnO C–S NWs for different gases (CO, C_6H_6, C_7H_8, and NO_2), and the energy band structure of the ZnO–SnO_2 heterojunction. This material is available free of charge via the Internet at http://pubs.acs.org.

■ AUTHOR INFORMATION

Corresponding Author

*E-mail: sangsub@inha.ac.kr.

Author Contributions

S.S.K. conceived the study, designed the experiments, and prepared the manuscript. S.-H.K. organized the atomic layer deposition process. S.-W.C., A.K., G.-J.S., and J.-H.K. performed the experiments. S.-W.C. and A.K. contributed equally to this work.

Notes

The authors declare no competing financial interest.

■ ACKNOWLEDGMENTS

This work was supported by a National Research Foundation of Korea (NRF) grant funded by the Korea government (MEST) (2012R1A2A2A01013899).

■ REFERENCES

(1) Law, M.; Kind, H.; Messer, B.; Kim, F.; Yang, P. Photochemical Sensing of NO_2 with SnO_2 Nanoribbon Nanosensors at Room Temperature. *Angew. Chem., Int. Ed.* **2002**, *41*, 2405−2408.
(2) Comini, E. Metal Oxide Nano-Crystals for Gas Sensing. *Anal. Chim. Acta* **2006**, *568*, 28−40.
(3) Field, L. L.; Zheng, J. P. Room-Temperature Low-Power Hydrogen Sensor Based on a Single Tin Dioxide Nanobelt. *Appl. Phys. Lett.* **2006**, *88*, 263102.
(4) Youn, S. K.; Ramgir, N.; Wang, C.; Subannajui, K.; Cimalla, V.; Zacharias, M. Catalyst-Free Growth of ZnO Nanowires Based on Topographical Confinement and Preferential Chemisorption and Their Use for Room Temperature CO Detection. *J. Phys. Chem. C* **2010**, *114*, 10092−10100.
(5) Polleux, J.; Gurlo, A.; Barsan, N.; Weimar, U.; Antonietti, M.; Niederberger, M. Template-free synthesis and assembly of single-crystalline tungsten oxide nanowires and their gas-sensing properties. *Angew. Chem.* **2005**, *44*, 1−6.
(6) Singh, N.; Ponzonib, A.; Gupta, R. K.; Leea, P. S.; Comini, E. Synthesis of In_2O_3−ZnO Core−Shell Nanowires and Their Application in Gas Sensing. *Sens. Actuators, B* **2011**, *160*, 1346−1351.
(7) Jang, Y.-G.; Kim, W.-S.; Kim, D.-H.; Hong, S.-H. J. Fabrication of Ga_2O_3/SnO_2 Core−Shell Nanowires and Their Ethanol Gas Sensing Properties. *Mater. Res.* **2011**, *25*, 2322−2327.
(8) Chen, Y.-J.; Xiao, G.; Wang, T.-S.; Zhang, F.; Ma, Y.; Gao, P.; Zhu, C.-L.; Zhang, E.; Xu, Z.; Li, Q. Synthesis and Enhanced Gas Sensing Properties of Crystalline CeO_2/TiO_2 Core/Shell Nanorods. *Sens. Actuators, B* **2011**, *156*, 867−874.
(9) Liu, X.; Zhang, J.; Guo, X.; Wang, S.; Wu, S. Core−Shell α−Fe_2O_3@SnO_2/Au Hybrid Structures and Their Enhanced Gas Sensing Properties. *RSC Adv.* **2012**, *2*, 1650−1655.
(10) Zhang, J.; Liu, X.; Wang, L.; Yang, T.; Guo, X.; Wu, S.; Wang, S.; Zhang, S. Synthesis and Gas Sensing Properties of α-Fe_2O_3@ZnO Core−Shell Nanospindles. *Nanotechnology* **2011**, *22*, 185501.
(11) Choi, S.-W.; Park, J. Y.; Kim, S. S. Synthesis of SnO_2−ZnO Core−Shell Nanofibers via a Novel Two-Step Process and Their Gas Sensing Properties. *Nanotechnology* **2009**, *20*, 465603.
(12) Rai, P.; Khan, R.; Raj, S.; Majhi, S. M.; Park, K.-K.; Yu, Y.-T.; Lee, I.-H.; Sekhar, P. K. Au@Cu_2O Core−Shell Nanoparticles as Chemiresistors for Gas Sensor Applications: Effect of Potential Barrier Modulation on the Sensing Performance. *Nanoscale* **2014**, *6*, 581−588.
(13) Park, J. Y.; Choi, S.-W.; Kim, S. S. A Model for the Enhancement of Gas Sensing Properties in SnO_2−ZnO Core−Shell Nanofibres. *J. Phys. D: Appl. Phys.* **2011**, *44*, 205403.
(14) Katoch, A.; Choi, S.-W.; Sun, G.-J.; Kim, S. S. An Approach to Detecting a Reducing Gas by Radial Modulation of Electron-Depleted Shells in Core−Shell Nanofibers. *J. Mater. Chem. A* **2013**, *1*, 13588−13596.
(15) Zheng, W.; Lu, X.; Wang, W.; Li, Z.; Zhang, H.; Wang, Y.; Wang, Z.; Wang, C. A highly sensitive and fast-responding sensor based on electrospun In_2O_3 nanofibers. *Sens. Actuators, B* **2009**, *142*, 61−65.
(16) Choi, S.-W.; Park, J. Y.; Kim, S. S. Growth Kinetics of Nanograins in Co_3O_4 Fibers. *Ceram. Interfaces* **2011**, *34*, 427−430.
(17) Choi, S.-W.; Park, J. Y.; Kim, S. S. Growth Behavior of Nanograins in NiO Fibers. *Mater. Chem. Phys.* **2011**, *127*, 16−20.
(18) Choi, S.-W.; Park, J. Y.; Kim, S. S. Growth Behavior and Sensing Properties of Nanograins in CuO Nanofibers. *Chem. Eng. J.* **2011**, *172*, 550−556.
(19) Park, J. Y.; Asokan, K.; Choi, S.-W.; Kim, S. S. Growth Kinetics of Nanograins in SnO_2 Fibers and Size Dependent Sensing Properties. *Sens. Actuators, B* **2011**, *152*, 254−260.
(20) Park, J. Y.; Choi, S.-W.; Kim, S. S. Junction-Tuned SnO_2 Nanowires and Their Sensing Properties. *J. Phys. Chem. C* **2011**, *115*, 12774−12781.
(21) Lee, D.-J.; Kim, K.-J.; Kim, S.-H.; Kwon, J.-Y.; Xu, J.; Kim, K.-B. Atomic Layer Deposition of Ti-Doped ZnO Films with Enhanced Electron Mobility. *J. Mater. Chem. C* **2013**, *1*, 4761−4769.
(22) Choi, S.-W.; Katoch, A.; Sun, G.-J.; Wu, P.; Kim, S. S. NO_2-Sensing Performance of SnO_2 Microrods by Functionalization of Ag Nanoparticles. *J. Mater. Chem. C* **2013**, *1*, 2834−2841.
(23) Sun, G.-J.; Choi, S.-W.; Katoch, A.; Wu, P.; Kim, S. S. Bi-Functional Mechanism of H_2S Detection using CuO−SnO_2 Nanowires. *J. Mater. Chem. C* **2013**, *1*, 5454−5462.
(24) Barsan, N.; Weimar, U. Understanding the Fundamental Principles of Metal Oxide Based Gas Sensors; the Example of CO Sensing with SnO_2 Sensors in the Presence of Humidity. *J. Phys.: Condens. Matter* **2003**, *15*, R813−R839.
(25) Sze, S. M. *Physics of Semiconductor Devices*, 2nd ed.; Wiley-Interscience: Singapore, 1936; Chapter 2, pp 63−132.
(26) Look, D. C. Recent Advances in ZnO Materials and Devices. *Mater. Sci. Eng., B* **2001**, *80*, 383−387.
(27) Jin, C.; Park, S.; Kim, H.; Lee, C. Ultrasensitive Multiple Networked Ga_2O_3-core/ZnO-Shell Nanorod Gas Sensors. *Sens. Actuators, B* **2012**, *161*, 223−228.
(28) Zheng, L.; Zheng, Y.; Chen, C.; Zhan, Y.; Lin, X.; Zheng, Q.; Wei, K.; Zhu, J. Network Structured SnO_2/ZnO Heterojunction Nanocatalyst with High Photocatalytic Activity. *Inorg. Chem.* **2009**, *48*, 1819−1825.
(29) Uddin, M. T.; Nicolas, Y.; Olivier, C.; Toupance, T.; Servant, L.; Müller, M. M.; Kleebe, H.-J.; Ziegler, J.; Jaegermann, W. Nanostructured SnO_2−ZnO Heterojunction Photocatalysts Showing Enhanced Photocatalytic Activity for the Degradation of Organic Dyes. *Inorg. Chem.* **2012**, *51*, 7764−7773.